Chapter 2

Computational Structural Biology of Opioid Receptors

Davide Provasi

Abstract

The publication of high-resolution structures for all of the opioid receptor subfamilies has unveiled exciting opportunities for mechanistic insight into the molecular mechanisms underlying the biology of nociception, reward, and higher cognitive functions, as well as promises for progress in several clinical areas such as pain management, physiological dependence, addiction, and mood disorders. To turn this promise into novel and improved therapeutic entities, however, this information needs to be supplemented with research strategies that explore the dynamic behavior of the proteins and their interactions with other receptors and ligands in their physiological environment.

Here we describe state-of-the-art molecular dynamics computational protocols, based on all-atom and coarse-grained modeling techniques, designed to estimate crucial thermodynamic and kinetic parameters describing the binding of small-molecule ligands and the formation of supramolecular complexes.

Key words All-atom models, Biased sampling techniques, Coarse-grained models, Dimerization, Ligand binding, Metadynamics, Molecular dynamics, Weighted histogram analysis method, Umbrella sampling

1 Introduction

One century ago M. von Laue won a Nobel Prize for envisioning how x-ray diffraction by crystals could be used to determine their structure to atomic resolution, and for inaugurating a powerful way to look directly at the finest details of matter. Soon, the same techniques were applied to small biological molecules (~1930s) and globular proteins (~1950s), ushering in a new era in the study of life sciences. In the last decade, despite the additional complexities characteristic of membrane protein crystallization, several technological advances have paved the way to the production of high-resolution crystal structures of G-protein coupled receptors (GPCRs) in general, and the opioid receptor (ORs) family in particular, providing priceless insight into the biology of these important proteins.

Santi M. Spampinato (ed.), *Opioid Receptors: Methods and Protocols*, Methods in Molecular Biology, vol. 1230,
DOI 10.1007/978-1-4939-1708-2_2,

While it is difficult to overestimate the importance of crystallography data for modern structural biology, high spatial resolution comes at a price.

First, except in very rare cases, biological macromolecules in cells are not in an ordered crystal phase. Thus, while crystal structures are invaluable information, the effects of the crystal packing and of the manipulations needed to produce such highly nonphysiological states need to be considered when formulating hypotheses about physiologically relevant cases. For example, the structure may be influenced by interactions with neighboring proteins across the boundary of the crystal unit cell and by the nonphysiological topology of the hydrophobic phases of lipids and detergents in the crystal.

Second, biological processes are intrinsically dynamic. Therefore, the static information obtained from crystallography must necessarily be supplemented by other techniques, including resonance spectroscopies (such as NMR, EPR, DEER, and ESR), fluorescence energy transfer (FRET, BRET), and computation. Despite the possibly lower spatial accuracy, these techniques can extend the exploration to the time domain and provide information on the dynamics of the system on different time scales.

The recent resolution of the first OR crystal structures [1–5] represents a long-awaited breakthrough in the structural biology of opioid signaling that had been based previously on indirect models produced by homology to other GPCRs. These data supply fundamental insight for the validation of existing hypotheses and the formulation of new ones regarding the biology and the pharmacology of pain, addiction, and mental disorders [6].

Of particular relevance to drug design and optimization are the mechanistic details governing ligand recognition and binding, as well as the flow of information from the orthosteric binding site to the intracellular region and the coupling to downstream signaling partners (G-protein and arrestins).

Equally important is the clarification of the role of supramolecular assemblies (dimers and oligomers) of ORs, as well as the functional role of both homodimers and heterodimers in opioid biology [7], in particular given the experimental evidence of pharmacologies specific to these complexes.

Undoubtedly, a complete picture will necessarily benefit from future OR crystals capturing the active forms of the proteins as well as from input from other structural and biophysical experiments. Nonetheless, computational techniques are valuable tools to supply accurate structural information and direct the design of molecules with specific binding selectivities (including heteromer selective compounds) and kinetics, with selective agonism in specific signaling pathways, or allosterically modulating the action of other drugs and endogenous ligands.

In the following sections, after a brief review of the OR crystal structures, we will describe how state-of-the-art computational methods can be used to complement crystal structure data to address some of the issues raised above. Specifically, we will describe molecular dynamics (MD) based computational protocols to study ligand binding to OR and to investigate the stability and kinetics of dimerization interfaces.

1.1 Opioid Crystal Structures

Crystal structures of representatives of each of the four opioid subfamilies (the μ-OR [1], δ-OR [4], κ-OR [2], and the nociceptin, or ORL-1 receptor [3], respectively MOR, DOR, KOR, and NOR) were simultaneously published in May 2012. These structures were made possible by a skilful combination of several technological breakthroughs, most specifically the reconstitution of the receptors in lipidic cubic phase [8, 9], and replacement of flexible regions of the protein with T4 lysozyme (T4L) [10] or fusion with the thermostabilized apocytochrome b562-RIL (BRIL) [11]. Binding of antagonist ligands was also used to stabilize inactive states, thereby reducing the conformational diversity of the proteins. These techniques have allowed an explosive increase in the number of GPCR crystals obtained in the last few years.

The murine (*mus musculus*) MOR was solved with a morphinan antagonist (BF0) covalently linked to K_{233} (5.39, in the Ballesteros-Weinstein notation, in which the helix number is followed by a residue index offset so that the most conserved residue is assigned the arbitrary position 50), to a resolution of 2.8 Å (PDB: 4DKL [1]); the human KOR was solved with a highly selective antagonist characterized by a very low dissociation rate (JDTic), to a resolution of 2.9 Å (PDB: 4DJH [2]). In these structures, the long intracellular loop (IC) 3 was substituted with T4L to enhance crystallization. Substitution of the BRIL bundle for the amino-terminal tail of the receptor afforded the crystallization of the human NOR bound to a mimetic of the endogenous peptide antagonist N/OFQ, to a 3.0 Å resolution (PDB: 4EA3 [3]). Finally, a first structure of the murine DOR was reported to a resolution of 3.4 Å (PDB: 4EJ4 [4]); the receptor is in complex with the highly selective morphinan antagonist naltrindole.

In February 2014, the Stevens group published a second, high resolution (1.8 Å, PDB: 4N6H [5]) structure of the human DOR receptor, also in complex with naltrindole, using the same BRIL substitution previously employed for the NOP structure.

Given the high average pairwise sequence identity among the ORs (71 % between the main subfamilies MOR, KOR, and DOR; 61 % between any of those and the NOR receptor), it does not come as a surprise that the transmembrane (TM) bundles exhibit few structural differences. This is also true for some of the less conserved regions; for instance, the long extracellular loop (EC) 2 also displays remarkable structural conservation, adopting a beta-sheet

conformation in all the crystals. Interestingly, the EC3, although shorter than EC2, could not be solved in the KOP structure and displays high temperature factors indicating high flexibility in all the crystals, and one single difference between the murine and the human gene of the DOP receptor in this region (an asparagine N instead of the aspartic acid side chain D290) [5] results in a different arrangement of the loop and in different chemical properties lining the extracellular rim of the binding pocket.

The importance of the region formed by EC3 and the extracellular ends of TM6 and TM7, as a "selectivity filter" for peptide and classic opioid binding, has been reported previously [12], and is now also highlighted by the binding poses of morphinan ligands in the OR crystal structures. In the framework of the address/message paradigm of opioid receptor pharmacology, classical opioids with a morphine-like scaffold bind towards this region of the binding pocket, whereas non-morphinan opioids are selected by addresses on the opposite side of the bundle (TM2/3). This demonstrates how an understanding of the flexible regions of the binding pocket is necessary for a thorough description of protein–ligand interactions.

Two of the OR crystal structures display interfaces between parallel receptors. It is tempting to infer from such evidence that similar dimeric arrangements would be formed also under physiological conditions, and may thus play a role in OR biology. The MOR crystal contains two different interfaces between the proteins. The first is a tightly packed arrangement, involving helices TM5 and 6 from each protomer, similar, albeit not identical, to an interface observed in the CXCR4 crystal (PDB: 3ODU, [13]). We note that, while TM5 has been implicated in dimerization of other GPCRs [14, 15], the conclusion of those experiments also revealed simultaneous involvement of TM4 and IC2 that are not at the interface in the crystal.

The MOR structure also reveals a second, less compact interface involving the extracellular halves of helices TM1 and 2 and the amphiphilic helix 8. A similar interface, comprising the same helices but featuring different contacts, appears in the KOR crystal. Notably, the participation of these helices in dimerization has also been reported in the past [15, 16].

Both DOR crystals display antiparallel dimers (i.e., complexes in which the extracellular region of one protomer is in contact with the intracellular region of the other), whose existence and functional relevance under physiological conditions is difficult to envisage.

Overall, it is clear that the interface data from the crystal structures, while representing an interesting additional piece of information regarding the putative features of the dimers, does not provide a clear answer to questions surrounding the detailed description of OR quaternary structure. We also note that a complete

characterization of the structural details of the interfaces is hardly enough to reach a full understanding of the biological significance of these receptor complexes. If, as data seem to support [7], several different interfaces are possible, their relative stability and the kinetic details of their formation will be critical to understanding the functional relevance of the dimeric states.

In the next sections we will review some of the computational methodologies that address the stability and kinetics of ligand binding and receptor oligomerization in a fully dynamic framework.

2 Materials

Computer programs implementing state-of-the-art algorithms for molecular dynamics and suitable for the simulations described in the following are widely available. The choice of which package to employ largely depends on the features of the available hardware resources and on personal preference, and will not be discussed here. Among the most popular codes we mention Gromacs (whose core development is currently taking place at the Department of Cellular and Molecular Biology, Uppsala University, and at the Stockholm Bioinformatics Center, Stockholm University, Sweden, www.gromacs.org); NAMD (developed by the Theoretical and Computational Biophysics Group at the University of Illinois at Urbana-Champaign, www.ks.uiuc.edu/Research/namd/); Amber (developed in an wide joint collaboration between groups at Rutgers University and several other institutions, www.ambermd.org); and Desmond (developed by D. E. Shaw Research, freely available for noncommercial use at www.deshawresearch.com and distributed by Schrödinger for commercial purposes). These packages natively implement the algorithms described in the following sections for umbrella sampling; some of them (e.g., NAMD, Desmond) also implement metadynamics. Umbrella sampling and metadynamics, along with a number of additional enhanced sampling strategies, can also be provided through the Plumed plugin code (www.plumed-code.org).

3 Methods

3.1 Reasonable Expectations for Binding Studies

Understanding the molecular mechanisms of ligand binding to ORs is an endeavor of paramount pharmacological relevance. Specifically, the interactions that drive binding selectivity (i.e., the ability of a molecule to bind to certain OR subtypes and not to others), efficacy (i.e., the resulting effect on signaling of the binding event), as well as different agonism profiles (i.e., selective activation of the G-protein vs. the arrestin pathways) are subjects of an intense research effort, with the final goal of designing molecular entities with optimal clinical efficiency.

To this end, the insight coming from crystal structures must be extended to the time domain, providing information on the binding pathways, kinetics, and thermodynamics, as well as the modulation induced by the ligand on the dynamics and on the conformational free-energy of the receptor.

When designing binding studies, it should be kept in mind that the structural details captured in the crystal structures reflect very specific conditions determined by the crystallogenesis. As noted above, (1) all the OR structures available so far were solved in complex with antagonist ligands; this stabilizes a homogeneous population of proteins in an inactive conformation, thereby increasing the probability of forming regular crystals. Moreover, (2) the presence of one specific ligand influences the binding pocket conformation; finally (3) the flexible regions of the protein (e.g., the EC and IC loops) can be influenced by crystal packing and interactions with fusion partners.

In computational terms, these three orders of problems translate into the impracticality of achieving sufficient sampling of the configurations relevant for the binding process. A second, unrelated, but critical problem is the accuracy of the model used to describe the molecular interactions between the protein, the ligand, and their environment. Thus, sampling and force-field accuracy still prevent MD-based methods from being a reliable *black-box* tool to predict quantitatively accurate absolute binding free-energies and to implement virtual screening techniques.

Nonetheless, if used properly, these techniques can offer valuable insight regarding key details of the binding process. While estimates of the binding thermodynamics can be obtained experimentally with relative ease, simulation affords the identification of binding pathways, intermediates, and structural details that can help rationalize the stability of the drug–protein complex and the kinetics of its formation, and modulate these crucial pharmacological parameters by molecular engineering.

3.2 System Preparation

Simulation results are obviously only reliable if the chemistry and the physics implemented in the model reflect the interactions relevant for the process being studied. A complete description of the interactions between the ligand and the protein requires quantum effects to be included in the simulation model. This, however, adds a layer of complexity to the simulations and drastically increases the computation cost, compromising the sampling of important degrees of freedom such a side chains rearrangements, solvation, and de-solvation of the ligand.

While the development of polarizable force fields could provide an optimal trade-off between model realism and computational cost (e.g., in cases where charge transfer interactions might be important [17]), these strategies are still not ripe for routine use in free-energy prediction studies, and a classical description seems the

most reasonable choice for the study of binding to opioid receptors (and to GPCRs in general). Within this approximation, however, extreme care must be taken to model the protein, the ligand, and the membrane lipids with high accuracy.

For small molecules, different parameterization strategies [18–20] have been proposed, requiring different levels of discretion and chemical savvy by the user. Recently, an automated strategy in the framework of the Charmm force field has been proposed and implemented in the ParamChem web server [20]. The approach automatically identifies the most accurate parameters in a curated set of molecular fragments, and assesses the reliability of the proposed parameters through a quantitative penalty score (*see* **Note 1**). Finally, protein preparation should follow standard guidelines for high-quality MD simulations (*see* **Note 2**).

3.3 Unbiased Binding Simulations

The recent increase in MD efficiency on both general and special purpose [21] machines has afforded simulations on time scales (~0.1 ms) that make possible the study of binding of ligands to proteins with unbiased simulations. Such simulations show that molecules placed in the simulation box beyond 20 Å from the protein surface can generally bind to the protein in approximately 1 μs [22–24]. Attempts to obtain numerical estimates of the kinetic and thermodynamic parameters from these simulations [22] have yielded results in qualitative agreement with experiments. The on-rate can be estimated modeling binding as a Poisson process, with probability

$$\mathrm{Prob}\left(N_t = n\right) = \frac{\exp\left(-k_{\mathrm{on}} c_{\mathrm{L}} t\right)\left(k_{\mathrm{on}} c_{\mathrm{L}} t\right)^n}{n!}$$

where N_t is the number of binding events that occur in time t, and c_{L} is the concentration of ligand molecules in the simulation box. The expected number of binding events in time t is $E(N_t) = c_L \times k_{\mathrm{on}} \times t$, so that an unbiased estimation of the Poisson rate is

$$\hat{k}_{\mathrm{on}} = \frac{N_t}{c_{\mathrm{L}} t}$$

that provides a way to estimate the rate based on the number of binding events. To put this value in context, however, we observe that the variance of the same estimator is given by

$$\frac{\mathrm{Var}\,\hat{k}_{\mathrm{on}}}{\hat{k}_{\mathrm{on}}^2} = \frac{1}{c_{\mathrm{L}} t \times \hat{k}_{\mathrm{on}}} = \frac{1}{N_t}$$

This relation reveals why very long simulations need to be performed with multiple copies of the ligand in the simulation box to increase the number of observed binding events and reduce the

relative variance (*see* **Note 3**). Using data from several simulations totaling to more than 120 μs, and observing 12 binding events [22] obtain a k_{on} for alprenolol on the β2-adrenergic receptor in good agreement with measured values. However, we note that such unbiased strategy can hardly be used to estimate ligand dissociation rates (*see* **Note 4**).

So far, no studies have been published on OR using this approach.

A promising alternative approach is to use unbiased simulations to produce data to construct Markov state models, and to effectively extend the description of the system at a coarse-grained level to the time scale of biological processes (see, for instance, reviews [25] and [26]). Within this framework, a large number (on the order of hundreds) of relatively short (on the order of 100 ns) simulations are analyzed to provide a coarse-grained description of the states sampled by the system, and to estimate transition probabilities between such states.

Markov state models have been applied with success to a number of binding studies, with varying aggregated simulation lengths (for instance 13 μs [27], 50 μs [28], 148 μs [29]). Since no application has been reported so far investigating the binding properties of ligands to GPCRs, we will not discuss them further, except for mentioning that they represent interesting and complementary alternatives to biased simulation strategies.

3.4 Biased Binding Simulations

Several biased techniques based on all-atom MD have been proposed and applied to study ligand binding and allow the estimation of affinities. A thorough description of computational methods to calculate absolute free-energies of binding is beyond the scope of this work, and we refer the interested reader to one of the many excellent reviews (see for instance [30]). Here, we will limit ourselves to some general considerations, a number of important principles that should be kept in mind while designing experiments for binding studies at OR, and a few illustrating examples.

Very broadly, practical computational protocols to calculate free-energy differences between two states can be classified as either (1) "alchemical" free-energy perturbation strategies, where the end points are connected by states with nonphysical interactions (e.g., states with scaled interactions between the ligand and the protein, as in decoupling methods) or (2) strategies where the ligand is physically separated from the receptor either by nonequilibrium pulling [31, 32] or by a direct calculation of a potential of mean force (PMF) by umbrella sampling [33, 34] or metadynamics [35].

While in their simpler form alchemical protocols are generally simpler to use, methods based on direct calculation of the PMF are better suited to incorporate improved sampling strategies for degrees of freedom such as protein and ligand flexibility and solvation [36]. In opioids, the long EL2 can act as a flexible lid, modulating the

accessibility to the orthosteric binding site. Moreover, while several important opioid ligands are rather rigid, ligand flexibility must be taken into account for larger small molecules and, especially, for peptides. Finally, it is worth noting that alchemical transformations of charged ligands involve additional complications to correctly account for electrostatic self-energy terms [33].

PMF-based methods, moreover, can identify physical intermediate states, supplying structural information about the binding pathways, which, as we have pointed out earlier, represent a good part of what MD-based computational binding studies are better suited for. As discussed above, binding of diffusible ligands to GPCRs in general and OR in particular most likely involves binding to intermediate entry states in the extracellular vestibule before the ligand can reach the orthosteric binding site in the TM bundle [22].

Among PMF-based strategies, metadynamics techniques allow to adaptively tune the necessary trade-off between the accuracy and scope of the sampling. In the absence of detailed experimental information about the binding process, it is possible to start with a qualitative [37] or low-resolution free-energy estimation to identify relevant states and conformations, followed by a refinement study.

There is no established protocol that has been shown to work better than others for the study of ligand binding to opioids. We will therefore describe the general ideas that can be used to address the technical requirements described above in the context of any PMF-based simulation strategy; the reader should keep in mind that these are only general guidelines.

The primary phase space direction to be sampled in association studies is clearly strongly correlated to the distance between the ligand and the binding site; this distance itself is thus one of the natural starting points for biased simulations.

The inclusion of collective variables that enhance the sampling of loop conformations or ligand internal degrees of freedom must be assessed based on the nature of the ligand and the receptor under study. For the former, a simple choice is to use just the distance between the center of mass of the loop itself and the center of mass of the protein (*see* **Note 5**). Once a low resolution description of the ligand binding pathway from the initial contact with the protein extracellular region towards the orthosteric binding pocket has been obtained, path variables [38, 39] can be used to obtain more accurate quantitative estimates for the free-energy difference along the binding process.

The techniques described above provide an efficient computational strategy to sample states with the ligand bound to different regions of the protein. To estimate the absolute binding affinity, the free-energy difference between protein-bound states and unbound states must be calculated, but because of the large volume of phase space corresponding to the latter, extensive sampling is difficult to achieve. On the other hand, when the ligand is sufficiently

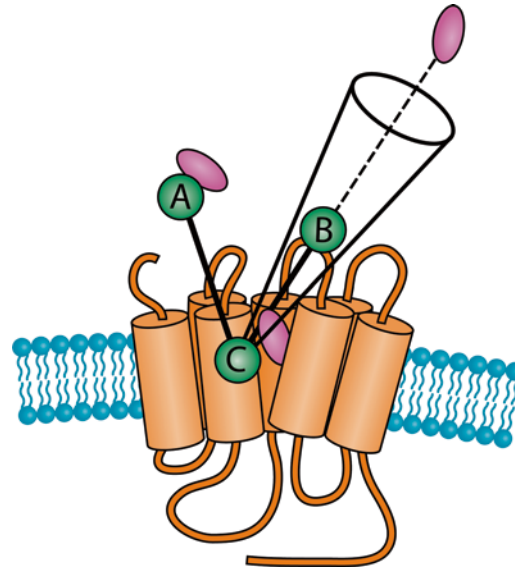

Fig. 1 Typical collective variables used in the study of ligand binding include (1) the distance between the ligand center of mass and the center of the orthosteric binding pocket (AC), (2) the distance between EL2 center of mass and the orthosteric binding pocket (BC), (3) the angle defined by the ligand, the orthosteric binding pocket, and EL2 (ACB). The limits of the conical region sampled to estimate the absolute free-energy difference to a reference state in the bulk solvent is also represented

distant from the protein surface, we expect the free-energy to be translationally invariant. We can thus overcome the bulk sampling problem by restricting the ligand to exploring a limited region of space that connects the bound state to an unbound reference. We report here the derivation for the case of a conic restraint used in [39] (Figs. 1 and 2), and refer the reader to the original formulation in [33] for the case of a cylindrical constraint. More advanced constraint shapes, such as funnel-shaped controls [40], have also been proposed. We note that similar expressions are also used to calculate the dimerization constant in Subheading 3.8.4.

A biased simulation is set up to obtain the free-energy $w(r)$ as a function of the distance between the ligand and the protein in the presence of additional external potentials constraining the ligand to be within a conical region containing the binding site and extending into the bulk. The binding affinity can be expressed in terms of the full potential of mean force $W(x)$ as

$$K^{-1} = \int_{\Sigma} dx e^{-(W(x)-W(x_0))/k_B T}$$

where x_0 is a reference position in the bulk, and Σ is the region of the phase space corresponding to the bound ligands. It is important to observe that the free-energy profile $W(x)$ is different from

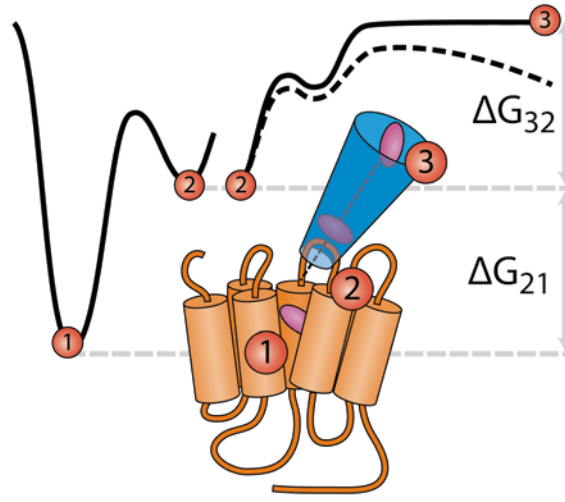

Fig. 2 Reconstruction of the full binding affinity using two separate metadynamics runs for the sampling of protein bound states (1, 2) and protein unbound states (2, 3). The unrestricted free-energy profile and the PMF reconstructed from the restrained simulation are represented as a *dashed* and a *solid line*, respectively

$w(r)$ because of the constraints limiting the explored region; specifically, switching to polar coordinates, the relation between the two profiles is given by,

$$e^{-W(r)/k_BT} = C\int_{\Omega} Jd\omega e^{-W(r,\omega)/k_BT}$$

where r is the polar distance, ω represents the polar angles, J is the Jacobian determinant, and the integral is calculated on the sampled region Ω. C is a normalization constant that can be fixed observing that invariance requires that W does not depend on the angular degrees of freedom ω at r_0. Thus

$$C^{-1} \simeq |\Omega| r_0^2 e^{W(x_0)/k_BT}$$

where $|\Omega|$ denotes the restraint's solid angle. Using this expression we can rewrite the relation between the full free-energy W and the sampled profile as

$$e^{-w(r)/k_BT} = \frac{1}{|\Omega| r_0^2}\int_{\Omega} Jd\omega e^{-[W(r,\omega)-W(r_0,\omega)]/k_BT}$$

so that the binding affinity can be expressed as

$$K^{-1} = |\Omega| r_0^2 \int_{\Sigma} dr e^{-w(r)/k_BT}$$

This constant reflects the thermodynamic equilibrium of the bimolecular reaction corresponding to the formation of a protein ligand complex Σ. To obtain a binding constant reflecting the concentration of ligands in the orthosteric binding pocket, the free-energy difference between the intermediate bound state Σ and the orthosteric site must be calculated. This can be easily accomplished using standard relations (Fig. 2), and expressing the full binding constant K_{31} as

$$K_{31}^{-1} = \frac{1}{[L]}\frac{p_1}{p_3} = \left(\frac{1}{[L]}\frac{p_2}{p_3}\right)\frac{p_1}{p_2} = K_{32}^{-1} e^{-\Delta G_{21}/k_B T}$$

where p_1 and p_3 are, respectively, the probabilities for the ligand to be in the binding pocket or in the bulk solvent, and p_2 is the probability of occupying the intermediate state Σ; $[L]$ is the ligand concentration, K_{32} is the binding constant to the intermediate state, and ΔG_{21} is the free-energy difference between the intermediate and bound state.

It should be kept in mind that any free-energy result is an estimate that crucially depends on the sampled molecular probability distributions, and thus that the statistical uncertainty of the final result should always be identified and reported (*see* **Note 6**). Finally, we call attention to the fact that the errors calculated only reflect the statistical uncertainty of the estimator used to derive the free-energy: additional contributions to the error due to insufficient sampling of relevant degrees of freedom should be assessed separately when possible, and pointed out during the discussion of the results.

3.5 Reasonable Expectations for Dimerization Studies

Despite large research effort, many of the fundamental questions regarding the physics and the biology of GPCR dimerization are still open. Our understanding of the nature of the physical forces that drive the dimerization remains incomplete, despite its practical importance in designing strategies to disrupt OR dimers [41], and in identifying the structural reasons of homo- and heterodimer selectivity.

Computational methods are promising tools to investigate the structural details of dimerization and oligomerization of membrane proteins, although several technical difficulties must be addressed and solved before a complete picture of the dimerization process can be successfully painted.

Solid experimental evidence shows that the characteristics of the lipid environment may play a role in the modulation GPCR function [42] and quaternary structure [43, 44]. First, this modulation can be mediated by specific binding of individual lipids or sterols to crevices on the outer surface of the TM region [45], effectively altering the shape and the physicochemical properties of

the protein surface and affecting the dimerization interface details and affinity. Second, membrane–protein interactions can modulate the elastic and rheological properties of the membrane, resulting in association strengths that could depend on membrane thickness [46–48], fluidity, and curvature [49]. Heterogeneous lipid compositions, moreover, introduce a new layer of complexity [50, 51].

Thus, while several implicit effective energy-function models have been proposed, membrane degrees of freedom must be explicitly included in the model to correctly reproduce the properties of the system on scales where the protein–protein distance is of the order of magnitude of a few lipid molecules [52, 53].

Luckily, in the last few years, reliable physical-based coarse-grained (CG) models reproducing the thermodynamics of several lipid phases and the partitioning of amino acids in polar and non-polar phases have been proposed (e.g., the MARTINI force-field [54]). These models have been used to start investigating, among others, several aspects of membrane protein dimerization and oligomerization. The strategy is based on an approximated 4-1 mapping of heavy atoms to coarse-grained beads, and on a careful parameterization of the nonbonded electrostatic and dispersion terms to reproduce thermodynamics experimental values. Models for lipids, sterols, sugars, and proteins are available [55]. The CG procedure accomplishes a significant reduction of the number of particles of the system, thus reducing the number of force computations necessary for the integration of the equations of motion and the computational cost of each of those calculations. Importantly, it also eliminates the fastest degrees of freedom in the system (such as fast bond stretching, small functional groups rotations, etc.) allowing a large increase in the integration time step without appreciable loss of accuracy.

3.6 System Setup for Coarse-Grained Dimeric Systems

All-atom protein models can be converted to CG representations with scripts (available on the Marrink lab website [56]) implementing the MARTINI [54] mapping.

Bonded parameters on the backbone pseudodihedrals are determined by the secondary structure of the input all-atom model and restrict the sampling to such structures. Changes in tertiary structures, albeit possible in principle, likely depend on details not accounted for within the approximations of the CG model, and their accuracy is therefore difficult to ascertain. For this reason, the desired conformation of the protein is chosen in advance, and the simulation is restricted to sample only small fluctuations around this conformation.

A convenient framework to do so is to add a network of elastic constraints to backbone beads pairs within a given distance [57]. The cutoff distance and the strength of the harmonic constraints have to be determined by comparing the RMSD fluctuations of the model with those of a corresponding all-atom system (*see* **Note 7**).

Several methods have been proposed and used to embed CG protein models in CG membranes. While self-assembly of the membrane around the protein [58] is convenient for complex membrane compositions and in cases where the positioning of the protein in the membrane is not known, other strategies are more efficient in simpler situations. The approach described by [59] involves a series of subsequent compression and equilibration steps of the lipids following an initial expansion of the membrane artificially increasing the spacing between the lipid molecules.

3.7 Unbiased Simulations of OR Dimerization

Unbiased simulations of GPCR diffusing freely in membrane bilayers have been proposed to investigate the dimerization process. Considerations similar to the ones expressed in discussing unbiased ligand binding studies also apply here.

Unbiased simulations can therefore only be effective in a very crowded regime (*see* **Note 8**). Furthermore, while dimer dissociation rates at given interfaces are difficult to obtain experimentally, single-molecule experiments [60] and biased simulations (see below) show that the dissociation is—in some cases—as slow as $k_{off} \sim 1.0\ s^{-1}$, so that we could not expect to see unbinding events in the time scale we can simulate.

Despite these limitations, unbiased strategies represent a very useful tool to generate hypothesis regarding putative dimerization interfaces [43, 61]. Special care should be taken when interpreting the results, making sure that sufficient statistics is accumulated by running replica simulations, and that the influence of the initial placing of the molecules has been ruled out, or accounted for.

3.8 Biased Simulations of OR Dimerization

3.8.1 Collective Variables

A complete description of the relative orientation of two proteins in a flat lipid bilayer requires seven values (Fig. 3): the relative tilting of the two protein axes is described by two polar and azimuthal angles for each protomer (θ_1, φ_1, θ_2, and φ_2), while the rotation of each protein around its axis is described by two more angles (α and β). In [61] the values of the six collective variables defining the relative orientation of the proteins were kept controlled with harmonic potentials [62]. While this assures complete control over the region of the phase space sampled by the simulation, the unbiasing procedure to extract the final free-energy needs to account for the restraints imposed using a (six-dimensional) generalization of the common weighted histogram analysis method (WHAM, see below). In flat membranes, the axis of GPCR molecules fluctuates around the normal of the membrane, so that the average values of θ_1, φ_1, θ_2, and φ_2 deviate only slightly from trivial values.

In this situation, the system is described by the distance and two angles, which specify completely the dimeric interface. Given the relative rigidity of the tertiary structure of the TM bundle, a computationally convenient way of specifying the angles α and β is to use the projection on the membrane plane of the angles defined

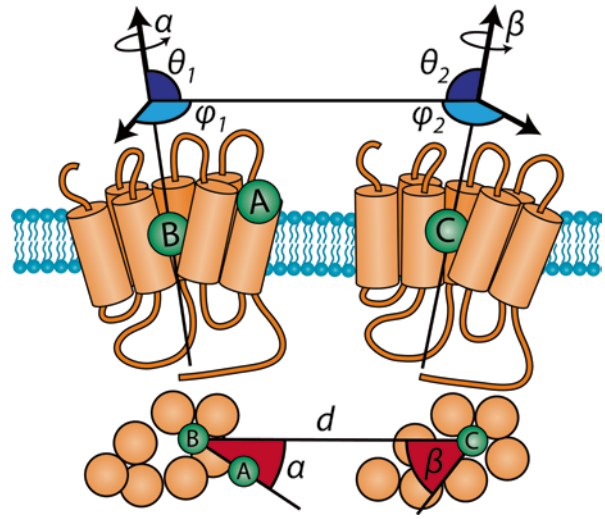

Fig. 2.3 Collective variables that specify the relative orientation of two protomers in the lipid bilayer. The absolute tilt of the protein principal axis is defined for each protomer by one polar and one azimuthal angles (θi and φi in *dark* and *light blue*, respectively). The description of the rotation of each protein around its principal axis requires two more angles (α and β)

by the center of mass of the two protomers and of one selected helix. Finally, the distance of the centers of mass d completes the definition of the relative position of the protomers.

The simulation protocol can be made more efficient by constraining the absolute position of the pair of proteins in the box. For example, the projection of the center of mass of one protomer on the membrane plane can be fixed to the center of the simulation box, and the second one can be allowed to move only along the xy diagonal [63].

3.8.2 Umbrella Sampling Simulations

Enhanced exploration of the relative distance can be efficiently achieved using umbrella sampling. Two different choices have been shown to give similar results. In one case (applied with success to a number of systems including opioids [63–65] and adrenergic receptors [66]) a relatively large number of simulations with strong harmonic restraints were run (approximately one point every 0.05 nm between 3.00 and 4.90 nm, with a harmonic restraint of 2,400 kcal/mol/nm^2). To achieve a proper overlap of the probability distributions, which crucially determines the accuracy of the resulting free-energy reconstruction, additional points might be inserted where the potential of mean force along the distance is particularly steep.

An alternative strategy was followed in [61]. Windows were spaced of 0.1 nm, and simulated with a much lower harmonic bias (~120 kcal/mol/nm^2), with additional windows run with

240 kcal/mol/nm^2 and 1,200 kcal/mol/nm^2. In each strategy, the windows were extended to approximately 0.8 μs each.

Different strategies have been experimented for the sampling of the relative orientation of the protomers described by the angles α and β; these can be restrained either with (1) additional harmonic restraints (as described in [61] and [65]), or with (2) square well potentials [63], or (3) their sampling can be enhanced with metadynamics [64, 66].

The first strategy only allows very limited remodeling of the dimeric interface, and therefore provides a viable method to assess the dimerization free-energy of a specific interface, defined by the equilibrium positions α_0 and β_0 of the harmonic umbrellas (*see* **Note 9**). This approach was applied to study the stability of the interfaces inferred in opioid crystal structures in [65], and to quantify the stability of putative rhodopsine interfaces [61] identified in self-assembly unbiased simulations.

Using weaker harmonic restraints, or a square-well potential, as in [63] in principle allows the system to explore refined interfaces, reaching a local minimum within the range of orientations allowed by the restraints. It is important to observe that the efficiency of such sampling is limited by the rotational diffusion constant and the length of the simulations (*see* **Note 10**).

To avoid this problem, metadynamics can be applied to the rotational degrees of freedom to accelerate the exploration, providing a converged estimation of the free-energy of different relative orientations of the two protomers. This strategy was applied to adrenergic receptors [64] and to ORs [66].

3.8.3 Reweighting

The biases introduced to enhance the sampling during the simulation must be properly accounted for when processing the data and extracting results. In the case of the simulation strategies described above, different approaches must be followed depending on the treatment of the orientation degrees of freedom.

In case (1), the restraints imposed on the system correspond to a three-dimensional umbrella sampling and can therefore be processed as usual by WHAM [67], Bennett Acceptance Ratio (BAR) [68], or Multistate BAR (MBAR) [69]. Since in this formulation only one umbrella corresponding to the studied interface α and β is applied along each orientation dimension, the unbiasing these in this case trivial, yielding

$$P_i^b(r) = Z^{-1} \int d\alpha d\beta \; P(\alpha, \beta, r) \; \mathrm{e}^{+U(\alpha-\alpha_0)/k_\mathrm{B}T} \mathrm{e}^{+U(\beta-\beta_0)/k_\mathrm{B}T}$$

where U is the usual harmonic umbrella, and Z a normalization constant. The reweighted probability distributions can be used in WHAM codes.

In metadynamics runs, a non-markovian bias is used to enhance the sampling of the relative orientation, so that WHAM or BAR

methods cannot be directly applied to remove the bias from the harmonic umbrellas along the distance degree of freedom. Rather, unbiased distance probabilities $P_{ib}(r)$ must be calculated for the distribution of the radial degree of freedom in the presence of the umbrella restraints, but removing the influence of the angular biases. This can be efficiently done using reweighting techniques developed to calculate Boltzmann probabilities from metadynamics simulations [70]. The usual WHAM or BAR techniques can then be applied to the resulting distributions.

3.8.4 Binding Affinity

Once a converged reweighted free-energy profile has been obtained, a formalism paralleling the one introduced for ligand binding can be applied to relate the free-energy as a function of the receptor distance to a binding constant. A standard dimerization free-energy can be calculated only after a reference state (or, equivalently, a scale) has been chosen. Following [71], we use the mole fraction scale, defining the dimerization constant K_X as the ratio of the mole fraction of dimeric and monomeric species in the membrane phase

$$K_X = \mathrm{e}^{-\Delta G^\circ_X / RT} = \frac{n_\mathrm{D} / n_\mathrm{T}}{\left(n_\mathrm{M} / n_\mathrm{T}\right)^2}$$

where n_D is the number of dimers, n_M the number of monomeric proteins, and n_T the total number of molecules (lipids and proteins) in the membrane compartment; the expression above also defines the free-energy ΔG°_X on this scale. Assuming diluted samples, the lipid concentration is greater than the protein concentration, so that the number of lipid molecules N_L is much bigger than $N_\mathrm{D} + N_\mathrm{M}$ and the total number of molecules $N_\mathrm{T} \sim N_\mathrm{L}$. With this assumption, we can express the mole fraction binding affinity K_X in terms of the binding affinity K_D on the surface concentration scale

$$K_X \simeq \frac{n_\mathrm{L}}{A} \times \frac{n_\mathrm{D} / A}{\left(n_\mathrm{M} / A\right)^2} = \frac{n_\mathrm{L}}{A} \times K_\mathrm{D}$$

where A is the surface area of the membrane. As we have seen in the ligand binding case, such binding affinity can be calculated from the calculated PMF, provided that the appropriate correction is included to account for the restraints imposed on the proteins during the simulation:

$$K_\mathrm{D} = \frac{|\Omega|}{\left(2\pi\right)^2} \int_\Sigma dr r \mathrm{e}^{-w(r)/k_\mathrm{B}T}$$

where $|\Omega| = |\Delta\alpha| \times |\Delta\beta|$ is now the 2D volume in the angle space sampled by the simulation, and the radial integral is calculated over the region of the PMF where the receptors are in contact.

The remarks made above regarding the importance of error

estimation are, of course, also valid for dimerization studies. Depending on the method chosen to reconstruct the free-energy $w(r)$, different strategies must be applied to the estimation of its variance (*see* **Note 11**) that can then be converted, using general statistical methods, to the error on the binding affinity K_D (*see* **Note 12**).

3.9 Summary and Outlook

Given the recent additions to the crystallographer toolbox, new self-labeling strategies for fluorescence spectroscopy, and the ever-increasing computational power available to a growing number of researchers, the outlook for the structural biology of OR looks bright.

For ligand binding, in particular, studies based on unbiased MD techniques, presented here, hold great promise for identifying not only orthosteric binding poses, but, most significantly, alternative and dynamically transient binding pockets relevant for allosteric modulation of the activation process. Qualitative information about the binding pathways and kinetics can also be obtained with this approach.

Unbinding events, however, cannot be sampled efficiently in standard MD simulations, and therefore converged quantitative estimates of binding free-energies can be obtained only from either biased simulations or enhanced strategies such as Markov state modeling techniques.

Single-molecule experiments, as well as new crystal structures, will greatly contribute to shedding light on the dimerization process, while the computational techniques described here will hopefully allow bridging the gap between high resolution structural data and single-molecule studies, allowing to compose a comprehensive picture of what complexes are sufficiently long-lived to contribute to the biology of opioid receptors.

To this end, some technical issues still need to be addressed. In particular, the conformational ensemble of flexible loops, which are likely to play a role in some of the proposed interfaces [7], is still inaccurate because of the simple approach used to describe backbone bonded interactions in the CG strategies presently in use.

4 Notes

1. Interactions at the opioid orthosteric site very often involve charge moieties. Paradigmatically, natural opium alkaloids (e.g., morphine and codeine) contain a weak acidic phenol ($pK_{a2} \sim 9.9$) and a strongly basic tertiary amine ($pK_{a1} \sim 8.0$) moiety; these molecules, along with a large class of narcotic analgesics are functionally basic compounds, forming a stable interaction in the binding site with the conserved aspartic acid side chain at position 3.32. For this, special care must be taken

in making sure that the ligand models accurately reflect the electrostatics. Inaccurate partial charges should be identified (by a careful analysis of the penalties), and remodeled by following the suggested parameterization strategy or by supplementing the fragment subset with additional molecules. Torsion terms with large penalties should also be checked against good ab initio quantum chemistry torsion scans, and modified as needed.

2. While crystal structures of constructs mimicking the interactions that stabilize the activated state of the receptor (e.g., with agonist ligands, G-protein partners [72] or nanobodies [73]) are well within the reach of available techniques, and will be fundamental to understand the interactions underlying the activation mechanism, there is not yet any direct experimental information about the details of the active states of OR receptors. Homology models based on other active GPCRs templates, as well as computational techniques designed to study the activation process using unbiased [74] and biased techniques [75–77], can be used to obtain models with binding pockets adapted to agonist binding, but the results must be interpreted with great care.
3. Typical settings [22] comprise up to 10 ligands, corresponding to concentrations as high as $c_L = 0.05$ M. Since for a large fraction of the simulation time several ligands are in contact with the membrane, a reduced value of $c_L t$ must be used to account for the effective concentration in the solvent phase.
4. Using the same Poisson approximation, the expected number of unbinding events in a simulation of length t is

$$\mathbb{K}(N_t) = k_{off} t$$

so that typical unbinding rates for opioids—e.g., for MOR [78], k_{off} are in the range ~0.02–2 min^{-1}—put the expected wait timescale for *one* unbinding event, $1/k_{off}$, significantly above the simulations length we can afford today even for fast dissociation compounds.
5. This is particularly effective in the case of well-structured loops (such as the EC2 one in opioid receptors), and was applied in the study of the binding of the classical antagonist naloxone in [39] (Fig. 1). More flexible loops should be described with collective variable adapted to the natural low-frequency dynamics, for example using principal components analysis (PCA) [79] or path-based [80] collective variables.
6. The most appropriate way of doing so depends, of course, on the particular computational method used. A detailed discussion of tests to control the convergence of umbrella sampling or metadynamics simulations is beyond the scope of this note,

and we refer the readers to one of the several review articles describing best practices in the field (see, for instance [81–83]). Special emphasis must be put in estimating the correlation in the data extracted from the simulations, and accounting for this in calculating the errors. Once the accuracies have been assessed for the different components contributing to the total binding affinity, error propagation can be used to obtain confidence intervals for the final estimate; in the case of the expression given above involving binding to one intermediate state, we obtain

$$\left(\frac{\delta K_{31}^{-1}}{K_{31}^{-1}}\right)^2 = \left(\frac{\delta K_{32}^{-1}}{K_{32}^{-1}}\right)^2 + \left(\frac{\delta \Delta G_{21}}{k_B T}\right)^2$$

When employing complex simulation strategies as the ones described here, in which the binding process is broken up in multiple steps, it is advisable to derive expressions of the final error in terms of the accuracy of each step, planning the length of each simulation so that the each one contributes similarly to the final variance, in order to avoid unbalanced scenarios.

7. For the study of GPCRs, where loops are more flexible than the transmembrane domain bundle, it is advisable to modulate the strength of the force constant depending on the secondary structure of the receptor residues. Typical values, obtained [63] by comparing a 50 ns long all-atom explicit simulation to several CG runs, are a cutoff $d_{\mathrm{Cut}} = 0.9$ nm, and elastic constants $k_{\mathrm{H}} = 1{,}000$ kJ/mol/nm^2 when both the residues involved are part of helical segments longer than two residues, or $k_{\mathrm{L}} = 250$ kJ/mol/nm^2 otherwise (i.e., coil, bend, hydrogen bonded turn, or other undefined structure).
8. We can obtain a very rough idea of the time scales involved by observing that the experimental 2D diffusion constant for ORs in membrane bilayers is of the order of $D \sim 0.1$ μm^2/s [84]. The average square displacement of each protein during the simulation time t is thus expected to be $\langle ds^2 \rangle \sim Dt$, so that to observe dimerization events we need a protein concentration $C = N_{\mathrm{P}}/A$ at least of the order of the critical concentration

$$C_0 \sim \frac{1}{2ds^2} \sim \frac{1}{2Dt_{\mathrm{eff}}} = \frac{1}{2 \times 4 \times D \times t}$$

where we have accounted for the fact that in CG simulations the effective physical time t_{eff} is roughly 4 times the simulation time. For a simulation length of, say, 100 μs, we see that we need a protein concentration larger than $C_0 \sim 1/(10^{-4}\ \mu\mathrm{m}^2)$. Assuming simple additive behavior, the area occupied by N_{P} proteins and N_{L} lipids can be easily expressed in terms of the

surface projection of one protein molecule (A_P) and the lipid unit area (A_L), so that the protein surface concentration in terms of the lipid:protein ratio $\rho = n_L / n_P$ is

$$C \sim \frac{1}{A_P + A_L \rho / 2}$$

Approximating $A_P \sim 7.0 \times 10^{-6}$ μm^2 and $A_L \sim 1.6 \times 10^{-6}$ μm^2, the constraint that $C > C_0$ entails that $\rho < \rho_0 = 110$.

9. It is useful to estimate the mean torque (i.e., the derivative of the free-energy with respect to the orientation degrees of freedom) exerted on the protomers by the harmonic restraints on α and β, and assess their influence in maintaining the interface. Large torques can signal instabilities of the studied arrangement and provide useful information regarding the closest metastable state. Since the free-energy estimate from each window is given by:

$$G_i = -k_B T \ln P_i^b(r,\alpha,\beta) - w_1(r,\alpha,\beta) + F_1$$

where i is the window index, P_{ib} is the biased probability distribution sampled by the simulation, w_i is the bias, and F_i is a constant resulting from the WHAM.

The mean force on each protomer is obtained by differentiating with respect to the corresponding angle. We can roughly estimate the torque in each window at the center of the bias and approximating the probability as a multivariate Gaussian:

$$P_i^b = \frac{e^{-(x-\mu)S^{-1}(x-\mu)/2}}{\sqrt{(2\pi)^3 \det S}}$$

where $x=(r, \alpha, \beta)$, μ is the mean vector, and S the covariance matrix, which can be easily calculated from the collective variables. Thus, the mean torque on the first protomer is:

$$\tau_\alpha(r_i) \simeq \frac{\partial G_i}{\partial \alpha} = -k_B T \sum_b (x-\mu)_b S^{-1}_{b\alpha}$$

Errors can be calculated by both block averaging, or by estimating errors on both μ and S and propagating.

Nonzero values of the torque reflect the tendency of the system to relax to a different interface, which is contrasted by the harmonic potentials applied to the angles. In other terms, the system could further minimize its free-energy by rearranging the contacts at the dimer interface.

10. The explored angular range can be estimated assuming a rotational diffusion in a flat potential, giving the order of magnitude estimate

$$\left\langle \delta\alpha^2 \right\rangle \sim tD_{\mathrm{R}}$$

For typical values of $D_{\mathrm{R}} \sim 10^4$ rad^2/s [85] and typical simulation length for CG simulations $t \sim 1$ μs we obtain $\langle \delta\alpha^2 \rangle \sim 0.01$ rad^2, corresponding to a change of ~5° in the orientation. Using wider windows without increasing the simulation length could result in significant undersampling of the orientation degrees of freedom.

11. Here we consider the error analyses for the combined use of metadynamics and umbrella sampling, since it represents an unusual simulation strategy. To provide a general framework for error analysis in this scenario, we use the approach described in [86], where the error on the one-dimensional free-energy $w(r)$ is expressed cumulatively in terms of the sample variance of the collective variable average in biased distribution

$$\mathrm{Var}\, w(r) = \left(k\Delta r\right)^2 \sum_{i=i(r)}^{M} \mathrm{Var}\, \hat{r}_i$$

where k is the elastic constant of the umbrella potential, and Δr is the spacing of the umbrella positions. These were assumed to be constant in writing the expression above, but equivalent expressions for the more general case can be obtained trivially. The variance of the average estimator can be expressed in terms of block average [87] when there is no other bias acting on the system. In the case where metadynamics is applied to enhance the angle sampling, block averages of the data does not lead to an unbiased estimator of the average.

An alternative approximated approach is to use instead the following expression

$$\hat{r}_i \simeq \sum_{\tau=0}^{T} g_\tau \left\langle r_i \right\rangle_\tau = \sum_{\tau=1}^{T} \frac{g_\tau}{\tau} \int_0^\tau dt \frac{\int dr\, r\, P_i(r,t)}{\int dr\, P_i(r,t)}$$

where T is the total length of the simulation, $P_i(r, t)$ is the biased distribution of r, at time t, after the bias on the angles has been removed by reweighting, and the weights g_τ are adjusted to account for the convergence of P_i. Empirical analysis of the convergence of the reweighting algorithm [88] shows

that convergence is linear with time, justifying the choice $g_\tau \sim \tau$. The variance can now be estimated simply by

$$\mathrm{Var}\,\hat{r}_i = \frac{\sum_{\tau=1}^{T} g_\tau \left(\hat{r}_i - r_{i\tau}\right)^2}{\sum_{\tau=1}^{T} g_\tau}$$

12. A useful approximation of the error on the dimerization rate can be obtained by expanding the PMF around the most stable state r_0, and approximating it as a harmonic interaction between the two proteins. Indicating with w_0 the depth of the PMF and with σ_r its spread we have that the PMF is $w(r) \sim w_0 + \sigma r^{-2} (r - r_0)^{-2}$ so that the integral can be calculated, and the resulting dimerization constant becomes:

$$K_D \sim \frac{|\Omega| \sigma_r^2}{(2\pi)^2} e^{-w_0 / k_B T}$$

so that the relative error on K_D can be expressed in terms of the uncertainty on the width and the depth of the PMF:

$$\left(\frac{\delta K_D}{K_D}\right)^2 = \left(\frac{2\delta\sigma_r}{\sigma_r}\right)^2 + \left(\frac{\delta w_0}{k_B T}\right)^2$$

With the protocols described here, the first term contributes only marginally to the overall error, which is dominated by the relative error on the depth of the PMF.

Acknowledgments

The author wishes to thank Jennifer Johnston and Sebastian Schneider for several stimulating discussions about GPCR computational biology and for the critical reading of the manuscript.

References

1. Manglik A, Kruse AC, Kobilka TS et al (2012) Crystal structure of the μ-opioid receptor bound to a morphinan antagonist. Nature 485:321–326
2. Wu H, Wacker D, Mileni M et al (2012) Structure of the human κ-opioid receptor in complex with JDTic. Nature 485:327–332
3. Thompson AA, Liu W, Chun E et al (2012) Structure of the nociceptin/orphanin FQ receptor in complex with a peptide mimetic. Nature 485:395–399
4. Granier S, Manglik A, Kruse AC et al (2012) Structure of the δ-opioid receptor bound to naltrindole. Nature 485:400–404
5. Fenalti G, Giguere PM, Katritch V et al (2014) Molecular control of δ-opioid receptor signalling. Nature 506:191–196

6. Filizola M, Devi LA (2012) Structural biology: how opioid drugs bind to receptors. Nature 485:314–317
7. Ferré S, Casadó V, Devi LA et al (2014) G protein-coupled receptor oligomerization revisited: functional and pharmacological perspectives. Pharmacol Rev 66:413–434
8. Landau EM, Rosenbusch JP (1996) Lipidic cubic phases: a novel concept for the crystallization of membrane proteins. Proc Natl Acad Sci U S A 93:14532–14535
9. Cherezov V (2011) Lipidic cubic phase technologies for membrane protein structural studies. Curr Opin Struct Biol 21:559–566
10. Zou Y, Weis WI, Kobilka BK (2012) N-terminal T4 lysozyme fusion facilitates crystallization of a G protein coupled receptor. PLoS One 7: e46039
11. Chun E, Thompson AA, Liu W et al (2012) Fusion partner toolchest for the stabilization and crystallization of G protein-coupled receptors. Structure 20:967–976
12. Bonner G, Meng F, Akil H (2000) Selectivity of mu-opioid receptor determined by interfacial residues near third extracellular loop. Eur J Pharmacol 403:37–44
13. Wu B, Chien EY, Mol CD et al (2010) Structures of the CXCR4 chemokine GPCR with small-molecule and cyclic peptide antagonists. Science 330:1066–10671
14. Hu J, Thor D, Zhou Y et al (2012) Structural aspects of M3 muscarinic acetylcholine receptor dimer formation and activation. FASEB J 26: 604–616
15. Huang J, Chen S, Zhang JJ et al (2013) Crystal structure of oligomeric beta1-adrenergic G protein-coupled receptors in ligand-free basal state. Nat Struct Mol Biol 20:419–425
16. Hu J, Hu K, Liu T et al (2013) Novel structural and functional insights into M3 muscarinic receptor dimer/oligomer formation. J Biol Chem 288:34777–34790
17. Dastmalchi S, Hamzeh-Mivehroud M, Ghafourian T et al (2008) Molecular modeling of histamine H3 receptor and QSAR studies on arylbenzofuran derived H3 antagonists. J Mol Graph Model 26:834–844
18. Jorgensen WL, Maxwell DS, Tirado-Rives J (1996) Development and testing of the OPLS all-atom force field on conformational energetics and properties of organic liquids. J Am Chem Soc 118:11225–11236
19. Wang J, Wolf RM, Caldwell JW et al (2004) Development and testing of a general amber force field. J Comput Chem 25:1157–1174
20. Vanommeslaeghe K, Hatcher E, Acharya C et al (2010) CHARMM general force field: a force field for drug-like molecules compatible with the CHARMM all-atom additive biological force fields. J Comput Chem 31:671–690
21. Shaw DE, Dror RO, Salmon JK, et al (2009) Millisecond-scale molecular dynamics simulation on Anton. In: Proceedings of the conference on high performance computing, networking, storage, and analysis. IEEE, Piscataway, pp. 1–11
22. Dror RO, Pan AC, Arlow DH et al (2011) Pathway and mechanism of drug binding to G-protein-coupled receptors. Proc Natl Acad Sci U S A 108:13118–13123
23. Shan Y, Kim ET, Eastwood MP et al (2011) How does a drug molecule find its target binding site? J Am Chem Soc 133:9181–9183
24. Dror RO, Green HF, Valant C et al (2013) Structural basis for modulation of a G-protein-coupled receptor by allosteric drugs. Nature 503:295–299
25. Noe F, Fischer S (2008) Transition networks for modeling the kinetics of conformational change in macromolecules. Curr Opin Struct Biol 18:154–162
26. Pande VS, Beauchamp K, Bowman GR (2010) Everything you wanted to know about Markov State Models but were afraid to ask. Methods 52:99–105
27. Silva D-A, Bowman GR, Sosa-Peinado A et al (2011) A role for both conformational selection and induced fit in ligand binding by the LAO protein. PLoS Comput Biol 7:e1002054
28. Buch I, Giorgino T, De Fabritiis G (2011) Complete reconstruction of an enzyme-inhibitor binding process by molecular dynamics simulations. Proc Natl Acad Sci U S A 108: 10184–10189
29. Bisignano P, Doerr S, Harvey MJ et al (2014) Kinetic characterization of fragment binding in AmpC β-lactamase by high-throughput molecular simulations. J Chem Inf Model 54: 362–366
30. Shirts MR (2012) Best practices in free energy calculations for drug design. Methods Mol Biol 819:425–467
31. Ytreberg F (2009) Absolute FKBP binding affinities obtained via nonequilibrium unbinding simulations. J Chem Phys 130:164906
32. Patel JS, Branduardi D, Masetti M et al (2011) Insights into ligand–protein binding from local mechanical response. J Chem Theory Comput 7:3368–3378
33. Woo H-J, Roux B (2005) Calculation of absolute protein-ligand binding free energy from computer simulation. Proc Natl Acad Sci U S A 102:6825–6830
34. Lee MS, Olson MA (2006) Calculation of absolute protein-ligand binding affinity using

path and endpoint approaches. Biophys J 90: 864–877
35. Gervasio FL, Laio A, Parrinello M (2005) Flexible docking in solution using metadynamics. J Am Chem Soc 127:2600–2607
36. Limongelli V, Marinelli L, Cosconati S et al (2012) Sampling protein motion and solvent effect during ligand binding. Proc Natl Acad Sci U S A 109:1467–1472
37. Soederhjelm P, Tribello GA, Parrinello M (2012) Locating binding poses in protein-ligand systems using reconnaissance metadynamics. Proc Natl Acad Sci U S A 109:5170–5175
38. Saladino G, Gauthier L, Bianciotto M et al (2012) Assessing the performance of metadynamics and path variables in predicting the binding free energies of p38 inhibitors. J Chem Theory Comput 8:1165–1170
39. Provasi D, Bortolato A, Filizola M (2009) Exploring molecular mechanisms of ligand recognition by opioid receptors with metadynamics. Biochemistry 48:10020–10029
40. Limongelli V, Bonomi M, Parrinello M (2013) Funnel metadynamics as accurate binding free-energy method. Proc Natl Acad Sci U S A 110: 6358–6363
41. O'Dowd BF, Ji X, O'Dowd PB (2012) Disruption of the mu-delta opioid receptor heteromer. Biochem Biophys Res Commun 422:556–560
42. Escribá PV, Wedegaertner PB, Goñi FM et al (2007) Lipid-protein interactions in GPCR-associated signaling. Biochim Biophys Acta 1768:836–852
43. Periole X, Huber T, Marrink SJ et al (2007) G protein-coupled receptors self-assemble in dynamics simulations of model bilayers. J Am Chem Soc 129:10126–10132
44. Goddard AD, Dijkman PM, Adamson RJ et al (2013) Lipid-dependent GPCR dimerization. Methods Cell Biol 117:341–357
45. Zheng H, Pearsall EA, Hurst DP et al (2012) Palmitoylation and membrane cholesterol stabilize μ-opioid receptor homodimerization and G protein coupling. BMC Cell Biol 13:6
46. Kusumi A, Hyde JS (1982) Spin-label saturation-transfer electron spin resonance detection of transient association of rhodopsin in reconstituted membranes. Biochemistry 21:5978–5983
47. Ryba NJP, Marsh D (1992) Protein rotational diffusion and lipid/protein interactions in recombinants of bovine rhodopsin with saturated diacylphosphatidylcholines of different chain lengths studied by conventional and saturation-transfer electron spin resonance. Biochemistry 31:7511–7518
48. Pearson LT, Chan SI, Lewis BA et al (1983) Pair distribution functions of bacteriorhodopsin and rhodopsin in model bilayers. Biophys J 43:167–174
49. Botelho AV, Huber T, Sakmar TP (2006) Curvature and hydrophobic forces drive oligomerization and modulate activity of rhodopsin in membranes. Biophys J 91:4464–4477
50. Barnett-Norris J, Lynch D, Reggio PH (2005) Lipids, lipid rafts and caveolae: their importance for GPCR signaling and their centrality to the endocannabinoid system. Life Sci 77: 1625–1639
51. Fallahi-Sichani M, Linderman JJ (2009) Lipid raft-mediated regulation of G-protein coupled receptor signaling by ligands which influence receptor dimerization: a computational study. PLoS One 4:e6604
52. Mondal S, Johnston JM, Wang H et al (2013) Membrane driven spatial organization of GPCRs. Sci Rep 3:2909
53. Mondal S, Khelashvili G, Johner N et al (2014) How the dynamic properties and functional mechanisms of GPCRs are modulated by their coupling to the membrane environment. Adv Exp Med Biol 796:55–74
54. Marrink SJ, Tieleman DP (2013) Perspective on the Martini model. Chem Soc Rev 42: 6801–6822
55. de Jong DH, Singh G, Bennett WFD et al (2013) Improved parameters for the martini coarse-grained protein force field. J Chem Theory Comp 9:687–697
56. Coarse grain force field for biomolecular simulations. Tools: proteins and bilayers. 18 Oct. 2013. http://md.chem.rug.nl/cgmartini/index.php/tools2/proteins-and-bilayers. Accessed 20 Mar 2014
57. Periole X, Cavalli M, Marrink SJ et al (2009) Combining an elastic network with a coarse-grained molecular force field: Structure, dynamics and intermolecular recognition. J Chem Theory Comput 5:2531–2543
58. Sansom MS, Scott KA, Bond PJ (2008) Coarse-grained simulation: a high-throughput computational approach to membrane proteins. Biochem Soc Trans 36:27–32
59. Kandt C, Ash WL, Tieleman DP (2007) Setting up and running molecular dynamics simulations of membrane proteins. Methods 41:475–488
60. Hern JA, Baig AH, Mashanov GI et al (2010) Formation and dissociation of M1 muscarinic receptor dimers seen by total internal reflection fluorescence imaging of single molecules. Proc Natl Acad Sci U S A 107:2693–2698

61. Periole X, Knepp AM, Sakmar TP et al (2012) Structural determinants of the supramolecular organization of G protein-coupled receptors in bilayers. J Am Chem Soc 134:10959–10965
62. Boresch S, Tettinger F, Leitgeb M et al (2003) Absolute binding free energies: a quantitative approach for their calculation. J Phys Chem B 107:9535
63. Provasi D, Johnston JM, Filizola M (2010) Lessons from free energy simulations of delta-opioid receptor homodimers involving the fourth transmembrane helix. Biochemistry 49: 6771–6776
64. Johnston JM, Aburi M, Provasi D et al (2011) Making structural sense of dimerization interfaces of delta opioid receptor homodimers. Biochemistry 50:1682–1690
65. Johnston JM, Filizola M (2014) Differential stability of the crystallographic interfaces of mu- and kappa-opioid receptors. PLoS One 9:e90694
66. Johnston JM, Wang H, Provasi D et al (2012) Assessing the relative stability of dimer interfaces in G protein-coupled receptors. PLoS Comput Biol 8:e1002649
67. Kumar S, Bouzida D, Swendsen RH et al (1992) The weighted histogram analysis method for free-energy calculations on biomolecules. I The method. J Comput Chem 13:1011–1021
68. Bennett CH (1976) Efficient estimation of free energy differences from Monte Carlo data. J Comput Phys 22:245–268
69. Shirts MR, Chodera JD (2008) Statistically optimal analysis of samples from multiple equilibrium states. J Chem Phys 129:129105
70. Bonomi M, Barducci A, Parrinello M (2009) Reconstructing the equilibrium Boltzmann distribution from well-tempered metadynamics. J Comput Chem 30:1615–1621
71. Fleming KG (2002) Standardizing the free energy change of transmembrane helix-helix interactions. J Mol Biol 323:563–571
72. Rasmussen SG, DeVree BT, Zou Y et al (2011) Crystal structure of the β2 adrenergic receptor-Gs protein complex. Nature 477:549–555
73. Rasmussen SG, Choi HJ, Fung JJ et al (2011) Structure of a nanobody-stabilized active state of the β2 adrenoceptor. Nature 469:175–180
74. Nygaard R, Zou Y, Dror RO et al (2013) The dynamic process of β2-adrenergic receptor activation. Cell 152:532–542
75. Provasi D, Artacho MC, Negri A et al (2011) Ligand-induced modulation of the free-energy landscape of G protein-coupled receptors explored by adaptive biasing techniques. PLoS Comput Biol 7:e1002193
76. Miao Y, Nichols SE, Gasper PM et al (2013) Activation and dynamic network of the M2 muscarinic receptor. Proc Natl Acad Sci U S A 110:10982–10987
77. Tikhonova IG, Selvam B, Ivetac A et al (2013) Simulations of biased agonists in the β2 adrenergic receptor with accelerated molecular dynamics. Biochemistry 52:5593–5603
78. Cassel JA, Daubert JD, DeHaven RN et al (2005) [3H]Alvimopan binding to the μ opioid receptor: comparative binding kinetics of opioid antagonists. Eur J Pharmacol 520: 29–36
79. Sutto L, D'Abramo M, Gervasio FL (2009) Comparing the efficiency of biased and unbiased molecular dynamics in reconstructing the free energy landscape of met-enkephalin. J Chem Theory Comp 6:3640–3646
80. Branduardi D, Gervasio FL, Parrinello M (2007) From A to B in free energy space. J Chem Phys 126:054103
81. Shirts MR, Mobley DL (2013) An introduction to best practices in free energy calculations. In: Monticelli L, Salonen E (eds) Biomolecular simulations: methods and protocols. Humana Press, New York, pp 271–311
82. Raiteri P, Laio A, Gervasio FL et al (2006) Efficient reconstruction of complex free energy landscapes by multiple walkers metadynamics. J Phys Chem B 110:3533–3539
83. Crespo Y, Marinelli F, Pietrucci F et al (2010) Metadynamics convergence law in a multidimensional system. Phys Rev E Stat Nonlin Soft Matter Phys 81:055701
84. Saulière-Nzeh NA, Millot C, Corbani M et al (2010) Agonist-selective dynamic compartmentalization of human Mu opioid receptor as revealed by resolutive FRAP analysis. J Biol Chem 285:14514–14520
85. Peters R, Cherry RJ (1982) Lateral and rotational diffusion of bacteriorhodopsin in lipid bilayers: experimental test of the Saffman-Delbrück equations. Proc Natl Acad Sci U S A 79:4317–4321
86. Zhu F, Hummer G (2012) Convergence and error estimation in free energy calculations using the weighted histogram analysis method. J Comput Chem 33:453–465
87. Flyvbjerg H, Petersen HG (1989) Error estimates on averages of correlated data. J Chem Phys 91:461–466
88. Berteotti A, Barducci A, Parrinello M (2011) Effect of urea on the β-hairpin conformational ensemble and protein denaturation mechanism. J Am Chem Soc 133:17200–17206

http://www.springer.com/978-1-4939-1707-5

Opioid Receptors
Methods and Protocols
Spampinato, S.M. (Ed.)
2015, XV, 326 p. 56 illus., 26 illus. in color., Hardcover
ISBN: 978-1-4939-1707-5
A product of Humana Press